JOURNAL OF MAGNETIC RESONANCE **133,** 368–373 (1998)
ARTICLE NO. MN981493

Quantitative ^{1}H MRI and MRS Microscopy of Individual V79 Lung Tumor Spheroids

Kevin R. Minard, Xiuling Guo, and Robert A. Wind[1]

Pacific Northwest National Laboratory, P.O. Box 999, MS K8-98, Richland, Washington 99352

Received May 12, 1997; revised March 18, 1998

In this Communication ^{1}H MRI and MRS microscopy experiments of individual V79 lung tumor spheroids with diameters between 550 and 650 μm are reported. The results have been used to determine the T_1, T_2, and D values as well as the concentrations of water, total choline, creatine/phosphocreatine, and mobile lipids in the viable rims and in the necrotic centers. © 1998 Academic Press

Key Words: **MR microscopy**; **tumor spheroids**; **metabolites.**

Multicellular tumor spheroids are used as *in vitro* models to study avascular tumor growth important for cancer research (*1–6*). In recent years, magnetic resonance (MR) microscopic imaging (MRI) has been used successfully to visualize the microscale heterogeneities characteristic of three-dimensional spheroid morphology in a non-invasive way, investigate regional differences in the distribution of intra- and inter-cellular water, and monitor the kinetics of tumor invasion (*6–9*). It is well known that besides MRI localized magnetic resonance spectroscopy (MRS) is extremely useful for the study of metabolic changes in diseased tissues and the effects of therapy, as resonance lines of several cellular compounds such as choline and mobile lipids are observed with intensity values that have been linked to tumorigenesis, increased proliferation of cells, cell apoptosis, and necrosis (*10–20*). Therefore it is a logical extension of the MR microscopy work on spheroids to investigate whether MRS will also display spectral features which can be associated with the specific properties of the various microregions within a spheroid. In a recent study the radial variation of proton spectra within individual spheroids was reported, and 1D proton chemical shift imaging was used for monitoring the effects of cyclocreatine (CY) treatment on large C6 glioma spheroids with a diameter of 1 mm or larger (*21*). Besides the CY resonance, the only resonance observed was that of the methylene chains present in mobile lipids. In this Communication, it is shown that high resolution proton spectra can be obtained in a relatively short time on regions in spheroids with a diameter as small as 0.55 mm, and that besides the lipid resonance, resonances arising from other metabolites are observed.

In the current study V79 lung tumor spheroids have been employed. These spheroids were cultured using the V79 cell line originally derived from Chinese hamster fibroblasts. The V79 cells were obtained from the American Tissue Culture Collection (ATCC) and carried as monolayers in Minimal Essential Media (MEM) containing Earle's salts. Media was supplemented with 10% fetal bovine serum, 200 μg/ml gentamicin, and 25 m*M* of HEPES buffer (pH 7.4). Spheroid growth was initiated by transferring cells from confluent monolayer cultures onto bacteriological plates. After 48 h, developing spheroids were transferred to a 500-ml spinner flask and stirred at 50 rpm. Spheroid diameters ranged between 500 and 900 μm after five days in the spinner flask. All cultures were incubated with 5% CO_2 in air at 37°C. Prior to each series of MR measurements, a single spheroid was selected from the spinner flask and placed into a solution containing phosphate-buffered saline (PBS) and 1 wt % low melting point agarose. The PBS solution was maintained just above the melting point of the agarose gel (~34°C), and a pipette was used to transfer the spheroid together with a small amount of liquid solution into a 1.3-mm-i.d. glass sample tube. Once inside, the sample tube was slowly rotated as the gel formed while the sample was allowed to cool to room temperature. This rotation ensured that the spheroid would be properly centered and completely encapsulated, thereby preventing undesired contact with the glass walls.

The experiments were performed using a Varian UNITY Plus imaging-spectrometer equipped with a standard 89-mm-vertical-bore magnet operating at 11.7 T. The microimaging probe was manufactured by D. G. Cory and co-workers (MIT) and contained a gradient coil package capable of generating magnetic field gradients up to 10 T/m along two orthogonal directions, and 2.5 T/m along the third (*22*). These large gradients made it possible to measure small diffusion coefficients, up to 100 times smaller than that of bulk water; see below. The NMR coil consisted of a five-turn horizontal solenoid with both an inner diameter and a length of 1.7 mm, which is an order of magnitude more sensitive than the larger 5-mm Helmholtz coil used in Ref. (*21*). This enhanced sensitivity made it possible to detect low metabolite concentrations not previously observed.

[1] To whom correspondence should be addressed.

1090-7807/98 $25.00

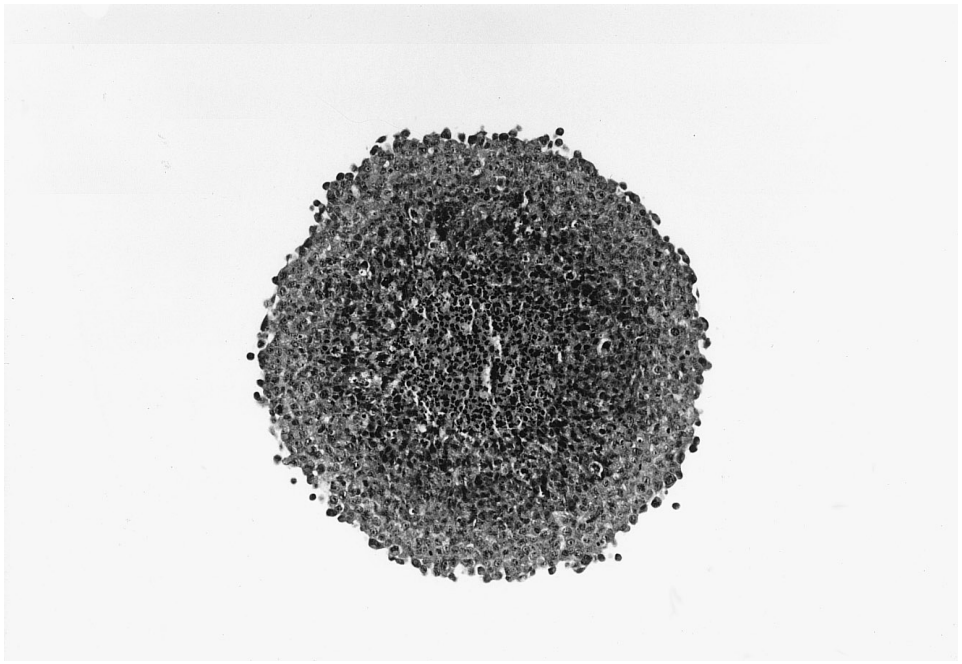

FIG. 1. Histologic section of a V79 lung tumor spheroid with a diameter of ~550 μm prior to the histology procedure. The actual diameter of the section shown in the figure is 470 μm.

In order to estimate the statistical variation of reported data, all experiments were repeated on five different spheroids having diameters between 550 and 650 μm. All measurements were performed at ambient temperature, 20.7 $\pm$ 0.1°C. At this temperature, no noticeable changes in MR images and/or acquired spectra were observed for at least 12 h. Magnetic resonance images were acquired using a standard two- and three-dimensional spin-echo sequence and localized spectroscopy was performed using PRESS (*23*). In the latter case, slice selection was performed with sinc RF pulses. Accurate placement of selected ROIs for localized spectroscopy was confirmed through incorporation of phase and frequency encoding gradients directly in the PRESS sequence, providing a two-dimensional image of the selected ROI. Localized T_1 and T_2 measurements were performed with Inversion Recovery and CPMG magnetization preparation periods in PRESS experiments, and localized diffusion measurements were performed with additional, motion-probing gradient pulses. Further experimental details are given in the figure captions.

Figure 1 shows a histologic section of a V79 spheroid with a diameter of ~550 μm, obtained by fixing the spheroid in formalin, embedding it in paraffin, cutting it into 5-μm-thick sections, and staining it with hematoxylin and eosin (*24*) (the actual spheroid diameter shown in Fig. 1 is decreased to 470 μm, which is the result of the histology procedure). An outer rim containing viable cells with enlarged nuclei (a typical property of malignant cells), and a necrotic center containing pyknotic cells (i.e., cells containing shrunken nuclei and in more or less advanced stages of degeneration) and cell fragments can be observed. Figure 2A shows the proton 3D image of a spheroid with a diameter of ~650 μm. The same microregions as those in the histologic section are observed, but with a considerably better contrast between the viable rim and the necrotic center. In fact, the center consists of a dark inner part, made up mainly of water and cell debris, and a bright intermediate region between the inner part and the rim, containing mostly still intact cells. These two central regions were observed in all V79 spheroids as well in EMT-6 spheroids studied by other investigators (*8*).

The basis for the observed image contrast was investigated by measuring T_1, T_2, and the diffusion coefficient D of the water in PRESS-selected volumes of 1 nl in the spheroid's rim, its intermediate zone, and its center, and in the agarose gel. Also, the water concentrations were determined by comparing the intensities (corrected for T_1, T_2, and diffusion losses) in the different microregions, and using the known concentration of 55.6 M of the water in the gel (in order to eliminate the effects of possible RF inhomogeneities, the measurements on the gel were performed after shifting the sample tube so that the ROI of the gel water was in the same location in the NMR coil as that of the spheroid earlier). The results are given in Table 1. In general the values found in the current study are comparable to those observed in spheroids derived from other cell lines (*6–9*). It was found that the spin–lattice and the spin–spin relaxation were monoexponential within experimental uncertainty. In contrast, multi-exponential attenuation in pulsed-field-gradient (PFG) diffusion experiments was observed, suggesting the presence of three distinct water compartments—

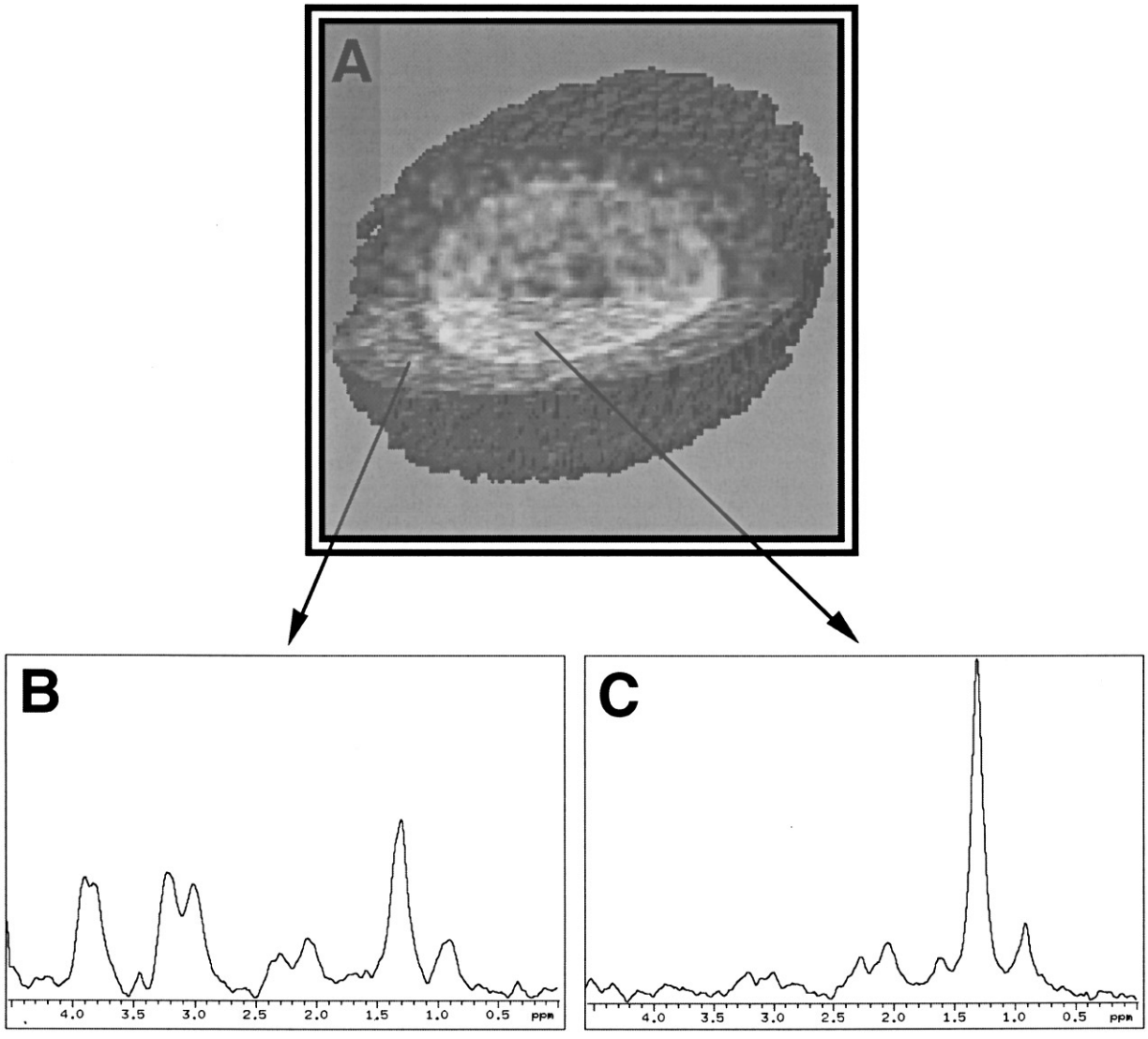

FIG. 2. ^{1}H 3D MR image and metabolite spectra of V79 lung tumor spheroids with a diameter of ~650 μm. (A) 3D image of the entire spheroid. The image was obtained after filtered reconstruction of the raw data within a 64 × 128 × 128 matrix; the spatial resolution is 13 μm in all directions. Raw data required 13.6 h to acquire using a standard 3D spin-echo sequence that employed four averages, a repetition time (TR) of 1.5 s, and an echo time (TE) of 27 ms. (B) Average water-suppressed ^{1}H spectrum of the spheroid rim. The selected rim volume is about 10 nl, TR = 1 s, TE = 10 ms, NEX = 3.6×10^3. An exponential line broadening of 20 Hz is applied. (C) Average water-suppressed ^{1}H spectrum of the spheroid center. The selected center volume is about 3 nl, NEX = 10.8×10^3; all other parameters are the same as those in (B).

each having significantly different mobility (slow, medium, and fast). Following Neeman *et al.* (*8*), we ascribe the compartments having medium and fast diffusion coefficients to the intra- and extracellular water, respectively. The third compartment, containing water which is 100 times less mobile than bulk water, and which is the largest in the intermediate zone, was observed after the magnetization from intra- and extracellular water had been completely destroyed. This slow diffusion suggests the presence of water in very small voids such as intra-nuclear compartments, and the fact that its fraction is the largest in the intermediate zone may be due to the presence of increased amounts of pyknotic nuclei in this region. However, more research is needed to confirm this conclusion. It can be noted that in contrast to our results, in Ref. (*8*) a single diffusion coefficient in the center is reported. This difference is probably due to the increased state of decomposition of the cells in the large necrotic center in the spheroid studied in Ref. (*8*), whereas the much smaller center in our spheroids still contains many intact cells; see Fig. 1. It can be concluded from the results given in Table 1 that the contrast in the image shown in Fig. 2A between the spheroid and the surrounding agarose gel is mainly due to diffusive differences, and that T_2 differences are mainly responsible for the contrast between the rim and the necrotic center.

TABLE 1
Average Regional Water Properties Measured at 20.7°C

	Rim	Intermediate zone	Center	Gel
T_1 (s)	1.5 ± 0.1	2.1 ± 0.1	2.1 ± 0.1	3.15 ± 0.03
T_2 (ms)	39 ± 6	91 ± 7	75 ± 10	121 ± 2
$D_0 \times 10^9$ (m^2/s)				1.980 ± 0.020
$D_s \times 10^9$ (m^2/s)	0.015 ± 0.010	0.018 ± 0.007	0.021 ± 0.006	
f_s	0.034 ± 0.021	0.103 ± 0.017	0.086 ± 0.013	
$D_m \times 10^9$ (m^2/s)	0.274 ± 0.045	0.252 ± 0.043	0.319 ± 0.055	
f_m	0.454 ± 0.105	0.370 ± 0.078	0.301 ± 0.089	
$D_f \times 10^9$ (m^2/s)	0.760 ± 0.030	0.890 ± 0.135	0.999 ± 0.050	
f_f	0.537 ± 0.073	0.544 ± 0.058	0.638 ± 0.075	
C_r (M)	30.5 ± 3.5	38.3 ± 3.7	37.1 ± 3.0	55.6

Note. D_0 denotes the bulk diffusion coefficient for water in the 1% agarose gel. D_s, D_m, and D_f represent the diffusion coefficients for the slow, medium, and fast water compartments present in the spheroids. Similarly, the volume fractions for the respective compartments are denoted by f_s, f_m, and f_f. Total region-specific molar concentrations for water are denoted by C_r. All reported values are denoted by the mean and standard deviations resulting from a statistical averages of values obtained from five different spheroids of similar size.

Again these results are in agreement with the findings in Refs. (*6–9*). Finally, it follows from Table 1 that the total water concentrations (intra- + inter-cellular) in the rim and the central regions are considerably less than the concentration of bulk water, resulting from the fact that a significant fraction of cell volume is occupied by relatively large cellular structures such as the nuclei and the membranes.

The heterogeneity characteristic of regional water properties is accompanied by comparable heterogeneity in observed metabolite spectra. This is illustrated in Figs. 2B and 2C, where the (water-suppressed) metabolite spectra acquired from the viable rim and the center are given. Both spectra are the average result of identical measurements performed on five different spheroids. It follows that spectra with a very acceptable signal-to-noise ratio can be acquired in a relatively short time, and that a good spectral resolution is obtained which is similar to that observed in regular tissues and in suspended cells (*13, 14, 19*). The spectral lines from the viable rim are slightly broader than those of the center, which is likely due to additional suceptibility broadenings occurring in this region (*25*). Several resonance lines can be distinguished. Elaborate spectral assignments are given elsewhere (*14, 19, 26, 27*); here we shall confine ourselves to a brief summary of the main features. The line at 3.8 ppm is due to protons in alkyl groups bound to oxygen or nitrogen and present in a variety of amino acids and other metabolites. The intensity at 3.2 ppm is a superposition of resonances originating from the methyl groups of various trimethylamine bearing metabolites such as free choline, phosphorylcholine, and glycerophosphorylcholine, present in, e.g., phospholipid precursors and degradation products. This line is usually called the total choline (Cho) line. The line at 3.0 ppm mainly arises from the methyl groups in the energy metabolites creatine and phosphocreatine (Cr/PCr), and the resonances at 2.3 and 2.1 ppm are due to methylene groups in glutamate, glutamine, and mobile lipids. The intensities at 1.3 and 0.9 ppm originate from methylene chains, respectively methyl end groups in triglycerides and other mobile lipids (we note that the line at 1.3 ppm could also be due to the methyl protons of lactate, but then a methylene line with a similar intensity would be present at 4.1 ppm, which is not observed).

Quantification of regional metabolite concentrations was performed using an approach much like that previously described for quantifying regional water concentrations. The primary difference is that metabolite relaxation times and molecular diffusion coefficients were not measured in each volume of interest chosen. Instead, measurements of these NMR parameters were performed using a volume large enough to encompass the entire spheroid. This ensured that all relaxation and diffusion data could be measured in an acceptable time. In addition, spectral deconvolution software on the Varian console was employed for quantifying all peak integrals (the same software was used to analyze the water data). As seen from the proton spectra shown, deconvolution was essential, particularly for quantitation of the partially overlapping lines of Cho and Cr/PCr.

The average T_1, T_2, D, and concentration values of the metabolite lines occurring at 3.2, 3.0, 1.3, and 0.9 ppm are summarized in Table 2. In general, all T_1 relaxation times were shorter than those measured for water, which allowed relatively short repetition times in the experiments. Also, because all metabolites displayed relatively long T_2 relaxation times, unavoidable T_2 losses in PRESS experiments were kept to a minimum, thereby allowing the twofold signal-to-noise advantage over stimulated-echo techniques to be fully realized. Diffusion-induced signal losses for both Cho and Cr/PCr typically appeared biexponential and reported diffusion coefficients correspond with the fastest components. In both cases, these were similar to recent values measured *in vivo* in the brain (*28, 29*).

TABLE 2
Average T_1, T_2, D, and Concentration (C) Values of Spheroid Metabolites

	Cho	Cr/PCr	Lipid CH_3	$N(CH_2)/N(CH_3)$
T_1 (s)	0.66 ± 0.05	0.45 ± 0.06	0.87 ± 0.07	
T_2 (ms)	151 ± 35	192 ± 40	77 ± 21	
$D \times 10^9$ (m^2/s)	0.11 ± 0.01	0.07 ± 0.02	0.0030 ± 0.0017	
C_{rim} (m*M*)	9.5 ± 3.7	14.7 ± 5.5	9.7 ± 5.6	3.0 ± 2.0
C_{center} (m*M*)	0.94 ± 0.70	2.3 ± 1.7	12.7 ± 5.1	8.0 ± 3.9

Note. The T_1, T_2, and D values were obtained using the spectra of the entire spheroid; the concentrations were determined separately on the rim and the center. As described in the text, $N(CH_2)/N(CH_3)$ represents the average ratio of $-(CH_2)_n-$ groups and methyl groups in observed lipids. All reported values are denoted by the mean and standard deviations resulting from a statistical average of values obtained from five different spheroids of similar size.

Likewise, measured diffusion coefficients for the methylene groups corresponded closely with recent findings obtained on cell suspensions (*30*). It was found that molecular diffusion was so slow for all metabolites that diffusion-induced signal losses were negligible. Together, these factors made it possible to acquire localized metabolite spectra with reasonable signal-to-noise ratios from 10-nl volumes in just 1 h. While such volumes could be chosen in the rim by taking advantage of the spheroid's spherical symmetry, smaller volumes between 3 and 5 nl were generally necessary in the center to avoid contributions from the rim. As a consequence, spectra of the center routinely required 3 h.

The metabolite concentrations were obtained again by comparing the integrated intensities of the various resonance lines with that of water in a ROI outside the spheroid. The concentrations were determined by assuming that the various compounds are homogeneously distributed within the rim and the center, and are corrected for T_1, T_2, and diffusive losses. Moreover, for the determination of the lipid concentration it has been assumed that on average a lipid contains two methyl groups (an average between triacylglycerides, phospholipids, and free fatty acids). As the amount of methylene groups per lipid is unknown, the average amount of $-(CH_2)_n-$ groups, giving rise to the peak at 1.3 ppm, per lipid chain is given instead. The following observations can be made: (i) The Cho and Cr/PCr concentrations are the largest in the viable rim, indicative of the proliferating properties of at least part of the cells in this area; (ii) the mobile lipid concentration is the largest in the necrotic center, presumably as a result of cellular decomposition in this region. The latter result is in agreement with that obtained by Kuesel *et al.* (*19*) and Schiffenbauer *et al.* (*21*), and also explains why in the latter reference Cho and Cr/PCr are not observed: the spheroids employed by these authors contained such large necrotic centers that the lipid signal dominates that of the other biochemicals (this observation was confirmed by us by performing ^{1}H MRS in V79 spheroids of different sizes).

It should be noted that in reality the concentrations of the various cellular compounds are larger than those given in Table 2, as these compounds are not homogeneously distributed throughout the rim or the center. For instance, taking the choline metabolite to be present in the intra-cellular water only, it follows from the total water molarity in the rim, 30.5 *M*, and the fraction of intra-cellular water in the rim, 0.454 (see Table 1), that its molarity becomes a factor of 4 larger than the value given in Table 2, i.e., becomes given by ~38 m*M*. A similar enhancement is obtained for the Cr/PCr concentration. The actual lipid molarity is more difficult to calculate. According to Refs. (*14–16*) these lipids are associated with the plasma membranes, and it is uncertain how much volume the lipids actually occupy.

In conclusion, microscopically localized proton spectroscopy provides a powerful basis for understanding the heterogeneity characteristic of three-dimensional spheroid morphology. ^{1}H metabolite spectra of a single spheroid and on volumes within a spheroid as small as 3 nl can be obtained in a relatively short measuring time, a few hours or less, even without utilizing special time-saving techniques developed in the literature (*31*). As these measurements can be performed on intact untreated spheroids, ^{1}H MRS can contribute to an improved understanding of the biological processes governing the evolution of these model tumor systems. Several improvements of the experiments reported in this Communication are possible. For instance, by inserting the spheroid into a perfusion system during the MR experiments (*8, 21, 32*), it should be possible to follow the spheroid growth or the effects of therapy in real time. Furthermore, by improving the volume selection technique more detailed information about the distribution of the various cellular compounds within the spheroid can be obtained. For instance, by selecting three-dimensional shells rather than rectangular volumes it can be investigated whether MRS can also be used to identify hypoxic areas and other layers of cells within the spheroid (*4, 5*), and to map the distribution of the various compounds within a spheroid in more detail. Finally, it is feasible that, also, ^{31}P MRS can be applied to single spheroids to study the distribution of, e.g., the energy metabolites. Currently all these improvements are under development in our laboratory.

ACKNOWLEDGMENTS

The authors thank Dr. Kevin M. Groch of the Pacific Northwest National Laboratory for his assistance with the culturing of the tumor spheroids, and Dr. Rodney A. Miller and Mrs. Katherine M. Gideon of Battelle, Preclinical Drug Development-Northwest Operations, for performing and evaluating the histology measurements. The Pacific Northwest National Laboratory is a multiprogram laboratory operated by Battelle Memorial Institute for the U.S. Department of Energy under Contract DE-AC06-76RLO 1830. X.G. was supported by the Associated Western Universities, Inc., Northwest Division, under Grant DE-FG06-89ER-75522 under the Department of Energy.

REFERENCES

1. J. P. Freyer, E. Tustanoff, A. J. Franko, and R. M. Sutherland, *J. Cell. Physiol.* **118,** 53 (1984).
2. P. L. Olive, and R. E. Durand, *Radiat. Res.* **101,** 94 (1985).
3. R. M. Sutherland, B. Sordat, J. Bamat, H. Gabbert, B. Bourrat, and W. Mueller-Klieser, *Cancer Res.* **46,** 5320 (1986).
4. W. Mueller-Klieser, *J. Cancer Res. Clin. Oncol.* **113,** 101 (1987).
5. E. J. Hall, "Radiobiology for the Radiologist," 3rd ed., Chap. 4, Lippincott, Philadelphia (1988).
6. R. M. Sutherland, *Science* **240,** 177 (1988).
7. L. O. Sillerud, J. P. Freyer, M. Neeman, and M. A. Mattingly, *Magn. Reson. Med.* **16,** 380 (1990).
8. M. Neeman, K. A. Jarrett, L. O. Sillerud, and J. P. Freyer, *Cancer Res.* **51,** 4072 (1991).
9. M. Brandl, J.-C. Tonn, K. Kotitschke, R. Goldbrunner, S. Kerkau, and A. Haase, *Magn. Res. Med.* **34,** 596 (1995).
10. P. F. Daly and J. S. Cohen, *Cancer Res.* **49,** 770 (1989).
11. M. Neeman, H. Eldar, E. Rushkin, and H. Degani, *Biochim. Biophys. Acta* **1052,** 255 (1990).
12. B. D. Ross, *NMR Biomed.* **5,** 215 (1992).
13. W. Negendank, *NMR Biomed.* **5,** 303, (1992).
14. C. E. Mountford, G. Grossman, G. Reid, and R. M. Fox, *Cancer Res.* **42,** 2270 (1982).
15. L. C. Wright, G. L. May, M. Dyne, and C. E. Mountford, *Fed. Eur. Biochem. Soc. Lett.* **203,** 164 (1986).
16. G. L. May, L. C. Wright, K. T. Holmes, P. G. Williams, I. C. P. Smith, P. E. Wright, R. M. Fox, and C. E. Mountford, *J. Biol. Chem.* **261,** 3048 (1986).
17. M. Stubbs, R. C. Coombes, J. R. Griffiths, R. J. Maxwell, L. M. Rodrigues, and B. A. Gusterson, *Br. J. Cancer* **61,** 258 (1990).
18. S. M. Cohen and L. B. Ellwein, *Science* **249,** 1007 (1990).
19. A. C. Kuesel, G. R. Sutherland, W. Halliday, and I. C. P. Smith, *NMR Biomed.* **7,** 49 (1994).
20. F. G. Blankenberg, R. W. Storrs, L. Naumovski, T. Goralski, and D. Spielman, *Blood* **87,** 1951 (1996).
21. Y. Schiffenbauer, C. Tempel, R. Abramovitch, G. Meir, and M. Neeman, *Cancer Res.* **55,** 153 (1995).
22. S.-M. Choi, X.-W. Tang, and D. G. Cory, *Int. J. Imaging Systems Technol.* **8,** 263 (1997).
23. P. A. Bottomly, *Ann. N. Y. Acad. Sci.* **508,** 333 (1987).
24. J. P. Freyer, and R. M. Sutherland *Cancer Res.* **46,** 3504 (1986).
25. P. W. Kuchel and B. T. Bulliman, *NMR Biomed.* **2,** 151 (1989).
26. W. Willker, J. Engelmann, A. Brand, and D. Leibfritz, *J. Magn. Reson. Anal.* **2,** 21 (1996).
27. L. L. Cheng, C. L. Lean, A. Bogdanova, S. Carter Wright Jr., J. L. Ackerman, T. J. Brady, and L. Garrido, *Magn. Reson. Med.* **36,** 653 (1996).
28. S. Posse, C. A. Cuenod, and D. Le Bihan, *Radiology* **188,** 719 (1993).
29. K. D. Merboldt, D. Horstermann, W. Hanicke, H. Bruhn, and J. Frahm, *Magn. Reson. Med.* **29,** 125 (1993).
30. P. Weybright, K. Millis, N. Campbell, D. G. Cory, and S. Singer, *Magn. Reson. Med.* **39,** 337 (1998).
31. D. W. Chakeres, and P. Schmalbrock, "Fundamentals of Magnetic Resonance Imaging," Williams & Wilkins, Baltimore (1992).
32. J. P. Freyer, N. H. Fink, P. L. Schor, J. R. Coulter, M. Neeman, and L. O. Sillerud, *NMR Biomed.* **3,** 195 (1990).